LIFE ASSESSMENT OF INITIATION FATIGUE CRACKS AROUND INCLUSIONS IN ROLLING FATIGUE

M. FREITAS* and D. FRANÇOIS**

Tests of fatigue crack initiation were carried out on a 52100 quenched and tempered rolling bearing steel, using a notched specimen tested under constant amplitude compression loading and correlations with assessment of crack formation life using Manson-Coffin and cyclic strain hardening laws are presented. Stresses and strains around inclusions in a Hertzian stress field produced by a rolling ball against a cylinder , were computed using a finite element bidimensional incremental elasto-plastic analysis. The strain distribution obtained allowed to explain the cyclic strain hardening of the martensitic steel around inclusions, as can be observed micrographically and the relative harmfulness of the various inclusions (alumina, nitride and spinel).
Assessment of fatigue crack initiation in rolling fatigue is presented using the strain distribution computed and the results of low cycle fatigue and compression tests. Two fatigue criteria are used to correlate these results with measured fatigue lifes of ball bearings as published in literature.
The agreement between predictions and test results is very promising.

Keywords : crack initiation, low cycle fatigue, rolling fatigue, bearing steel

INTRODUCTION

The fatigue crack initiation which takes place at the surface can be predicted by the consideration of a tiny fictitious specimen which consumes its life time when submitted to the local cyclic plastic deformation in a strain concentration region (1). The fatigue initiation time is then a function of the local strain range itself depending upon the cycle behaviour of the material and the plastic fatigue life.

In rolling fatigue the role of inclusions is of prime importance (2,3, 4). Micrographic observations reveal without ambiguity that the fatigue cracks are nucleated at inclusions below the surface (2,5), in the region where the tangential stress is maximum (according to Hertz studies (6)), these cracks are associated with structural modifications of the martensite, white phases and butterflies, inclined at 45° with respect to the surface (7,8).

* Cemul-Centro de Mecânica e Materiais da Universidade Técnica de Lisboa
Ed. IST, Av. Rovisco Pais, 1096 Lisboa Codex, Portugal
** École Centrale des Arts et Manufactures
Grande Voie des Vignes, 92290 Chatenay-Malabry, França

The interpretation of the phenomena must be related to the mechanical properties both of the inclusions and thus to their chemical nature, to their shape and dimensions and of the martensitic matrix. In fact, as the matrix and the inclusions have different elastic properties a stress concentration region arrises, leading to local plastic strains.

Attempts made to rationalise the classification of the inclusions according to their harmfulness are not adequate, (9, 10), because they don't take into account the mechanical properties of the inclusions nor the cyclic behaviour of the matrix. Quantitatively the phenomena has not been explained. The present study used the approach for prediction of the fatigue crack initiation in a strain concentration region, linking the crack initiation around inclusions in rolling fatigue with local plastic behaviour of the matrix in cyclic conditions.

The authors (11), using low cycle fatigue concepts, could predict the harmfulness of the various inclusions; a first approach to the crack initiation was used with a modification of Manson-Coffin law, (12) to take into account the existence of a high mean compression stress and strain. In the present work tests are made to verify this criteria and another fatigue criteria is used to calculate with more accuracy the crack initiation life.

MATERIAL TESTED

A 52100 rolling bearing steel was studied. It was slag remelted, giving a low inclusion count. The chemical composition is given in Table I.

The steel was austenized at 850°C for 20 min. in a neutral salt bath, quenched in oil at 20°C and annealed at 180°C for 2 hours and then air cooled.

The hardness obtained was HR_C *61.5*. The residual austenite fraction was 10 percent.

PLASTIC FATIGUE TESTS

Plastic fatigue tests were carried out with two kinds of specimens : smooth and notched ones.

Smooth Specimens

Smooth specimens used were hourglass shaped with a minimum diameter of *5 mm* and a radius of curvature of *30 mm*.

Equipment and Procedure. The fatigue tests were carried out on a *250 KN* servohydraulic MAYES fatigue machine, using total diametral strain control. The diametral strain was measured with a LVDT extensometer. The cycles were sinusoidal around zero mean strain at a frequency of *0.01* to *1Hz*. The load and the displacement were continuously recorded. The following tests were performed:

- fatigue tests at a prescribed strain range until fracture
- fatigue tests at increasing levels of strain ranges
- fatigue tests using programmed blocks of increasing and decreasing strain ranges.

Results. Hysteresis loop were obtained with an increasing maximum stress corresponding to a cyclic strain hardening behaviour obeying the law:

$$\Delta\sigma/2 = 5790\ (\Delta\varepsilon_p/2)^{0.137}$$

the stress being expressed in *MPa*, and $\Delta\varepsilon_p$ being the amplitude of the plastic strain. This is shown on figure 1 which was obtained by the three methods listed above.

Figure 2 shows the fatigue life, the strain amplitude being divided in the plastic and the elastic strain amplitudes. The corresponding law is:

$$\Delta\varepsilon/2 = 0.0073\ (2N_f)^{-0.36} + 0.0145\ (2N_f)^{-0.062}$$

Notched Specimens

Notched specimens used were cylindrical shaped with a diameter of *20mm*, the notch having a minimum diameter of *20 mm* and a radius of curvature of *2.5 mm*.

Equipment and Procedure. The fatigue tests were carried out on a *250 KN* servohydraulic MAYES fatigue machine, using load control. The cycles were sinusoidal with a mean compression load, at a frequency of *5* to *10 Hz*. For crack initiation detection an optical method (amplification 30 times) was used. After crack initiation detection the test was stopped, because fracture can not occur with compression loads.

Results. To determine the stress concentration factor K_t, we consider the perfect elastic behaviour:

$$K_t = \Delta\sigma_{max}/\Delta\sigma_{nom}$$

and as we are in fatigue conditions we used the Neuber's empirical formula for the stress concentration factor in fatigue K_f^N :

$$K_f^N = 1 + \frac{K_t - 1}{1 + \sqrt{A/\rho}}$$

where A is *0.01* for martensitic steels and ρ is the radius of curvature at the notch *(2.5 mm)*.

Based now on the Neuber rule (13), $K_t^2 = K_\sigma \cdot K_\varepsilon$, where $K_\sigma = \Delta\sigma/\Delta\sigma_{nom}$ is the stress concentration factor in the elastic-plastic domain and $K_\varepsilon = \Delta\varepsilon/\Delta\varepsilon_{nom}$ is the strain concentration factor, and according to the Morrow and al (14) modification that replaces K_t with K_f, $K_f^2 = K_\sigma \cdot K_\varepsilon$, we can compute $\Delta\sigma$ and $\Delta\varepsilon$ at the notch root using this formula and the cyclic stress strain curve of the material.

The linear relation between the stress range at the notch root $(\Delta\sigma)$ and the number of cycles to crack initiation *(Ni)* was found to be:

$$\Delta\sigma = 3706\ (Ni)^{-0.023}$$

the stress being expressed in *MPa*. Figure 3 represents this linear relation and the predictions of crack initiation using a modification of Manson-Coffin law, to take into account the existence of a non zero mean stress and strain. The correlation is very promising, if we consider that the crack initiation method used was an optical one.

ANALYSIS OF CRACK INITIATION IN ROLLING FATIGUE

Crack initiation around inclusions in rolling fatigue is always associated with metallurgical transformations caused by the plastic strain cycling in a compression state of stress (7,8). So we decided to make an elastic-plastic computation of the strain distribution around inclusions, using the cyclic stress-strain curve for the martensitic matrix and a perfect elastic behaviour of the inclusion.

Calculations were made into two steps : first, the stress and strain distribution of rolling fatigue was computed according to Hertz formulation. The maximum stress region is located below the contact area at a distance which is a function of the applied load and of the radius of curvature of the bodies in contact. Hertzian's stresses are a function of the load and of the contact area defining the maximum imposed pressure :

$$P_{max} = (2q\Delta/\pi)^{1/2} /\Delta$$

with

$$\Delta = 4R\ (1 - \nu^2)/E$$

q being the load on the ball and R the radius, ν Poisson's ratio and E Young's modulus.

The variation of the stresses in the region where the shear stress is maximum is shown on figure 4 as a function of the horizontal distance to the ball. They represent the boundary conditions which will be imposed to a small zone of the matrix containing a fatigue initiating inclusion of average size $r = 0.005\ mm$. A numerical analysis is then carried out using finite element program allowing elastic-plastic behaviour.

Results of the Numerical Analysis

The results of the computation showed that the maximum plastic strain is found at the interface between the inclusion and the matrix and the map of the cumulative plastic deformations during the loading for a ball rolling from left to right allows to explain the dissymetry of metallurgical transformations associated with the cracks (11, 15).

For a ball pressure equal to $3500\ MPa$ the strain range reaches 0.13% for an alumina inclusion, a value which is higher than the strain range corresponding to the stress range according to the cyclic stress strain law. The difference is due to the cumulative nature of the plastic strain.

Tables II and III represent respectively for $P_{max} = 3500\ MPa$ and $P_{max} = 5000\ MPa$ and an alumina inclusion the stresses at the point in the interface matrix inclusion where the plastic strain ranges is maximum. We can now compute the number of cycles to crack initiation using the modified Manson-Coffin law of figure 3.

We obtain for $P_{max} = 3500\ MPa$, $Ni = 260 \times 10^6$ cycles and for $P_{max} = 5000\ MPa$, $Ni = 8.5 \times 10^6$ cycles.

Correlations with Fatigue Life

When using Manson-Coffin law we must apply the concept of equivalent stress for computing $\Delta\sigma_{eq}$ and correlate with tests where the stress is uniaxial. Some authors contest these criteria, specially when stresses are not in phase during a cycle of fatigue, as it is the case in a

rolling fatigue cycle : as can be seen in figure 4, the maximum of τ_{xy} is obtained before the maximum of σ_{yy}.

So, we decided to verify these calculations using another fatigue criteria, due to Dang Van (16) where in a diagram of the shear stress $\tau(t)$ as a function of the hydrostatic stress $p(t)$, the endurance limit is defined by two lines symetrical with respect to the hydrostatic axis. Drawing $(\tau(t), p(t))$ for each point of the stabilised cycle of loading, we should obtain the fatigue limit of the component when the cycle reaches this intrinsic curve.

From the elastoplastic finite elements computation we look for the plane at the interface between the matrix and the inclusion where the shear stress is maximum. At any time on that particular plane the shear stress $\tau(t)$ is taken as the difference between the maximum and the average shear stress. Figures 6 and 7, respectively drawn for $p_{max} = 3500\ MPa$ and $p_{max} = 5000\ MPa$, the corresponding values being given in Tables IV and V, show the stabilized cycles thus obtained. The fatigue limit intrinsic curves are defined by two points deduced from the tests previously described (fig. 5). In tension compression tests the fatigue limit corresponding to 10^8 cycles was measured: a value of $\Delta\Sigma/2 = 995\ MPa$ was obtained giving a maximum shear stress amplitude τ equal to $497.5\ MPa$ and an hydrostatic stress amplitude p equal to $331.6\ MPa$. In repeated compression tests a value of $\Delta\Sigma = -2426\ MPa$ was obtained giving a maximum shear stress amplitude τ equal to $1213\ MPa$ and an hydrostatic stress amplitude p equal to $-808.6\ MPa$. The intrinsic fatigue limit curve is supposed to be a straight line going through these two experimental points on the τ, p diagram. Figures 6 and 7 shows that the 10^8 cycles fatigue limit should be between $p_{max} = 3500$ and $p_{max} = 5000\ MPa$, which is in good agreement with the previous criteria used.

DISCUSSION AND CONCLUSIONS

Results of rolling bearing tests of 52000 bearing steel are numerous in the literature: but only a few allow a precise identification of the fatigue crack initiation inclusion leading to fatigue failure. In general, the authors analyse rolling bearing tests by Weibull lines for different steel-making practices resulting in different inclusion contents, defined by the largest percentage of an inclusion type.

We have retained the results of two authors (17, 18) where the correlation between fatigue life and inclusion content is the best. Table VI is the correlation between the prediction of crack initiation life which we obtain and results of rolling bearing tests.

Despite the limitations of the model used in this study (plane strain conditions, perfect elastic inclusions, etc) and despite the results of the statistical distribution of the results of bearing steel tests the correlation obtained is very promising.

BIBLIOGRAPHY

1. Baus, A., Lieurade, H.P. and Sanz, G. in Flaw Growth and Fracture, ASTM STP 631, American Society for Testing and Materials, 1977, pp 96-111.

2. Tricot, R. and al., Metal Engineering Quarterly, 12, May 1972, pp 39.

3. Vincent L., and al., Mémoires Scientifiques de la Revue de Métallurgie, Mai 1976, pp 303.

4. Bearing Steels : the rating of non metallic inclusions, ASTM STP 575, American Society for Testing and Materials, 1975.

5. Styry, H., Fatigue Strength of Ball Bearing Races and Heat Treated 52100 Steel Specimens, Proceedings ASTM 51, pp 682.

6. Hertz, H., Gesammelte Werke, Vol. 1, Leipzig 1895.

7. Osterlund, R., Vincent, L. and al., Scandinavian Journal of Metallurgy, 11, 23-32, 1982.

8. Freitas, M. and François, D., Scripta Metallurgica, Vol. 17, p 683, 1983.

9. Brooksbank, D., Andrews, K., Journal of the Iron and Steel Institute, June 1968, April 1969, April 1972.

10. Kiessling, R., Non Metallic Inclusions in Steel, part. III, The Iron and Steel Institute, 1968.

11. Freitas, M. and François, D., Communication to "2nd Int. Elastic-Plastic Symposium" ASTM Philadelphie (Oct. 1981).

12. Antolovich, S.D., and al., Notch Fatigue Life Prediction using Smooth Bar Fatigue Data, Fracture 1977, Vol. 2, I.C.F. 4.

13. Neuber, H., Journal of Applied Mechanics, Vol. 28, nº 4, December 1961, pp 544-560.

14. Morrow, J., Topper, T., Wetzed, R., Laboratory Simulation of Structural Fatigue Behaciour, ASTM STP 462, 1968, pp74-91.

15. Freitas, M., Amorçage de Fissures de Fatigue autour des Inclusions dans les aciers de roulement, thèse de Docteur d'Etat, UTC, France, 1982.

16. Dang Van, R., Sur la Resistance à la Fatigue des Métaux, Sciences et Techniques de l'Armement, Mémoires d'Artillerie, 3ème fascicule pp 647-720.

17. Okamoto, K., Shiko, S., Nippon Steel Technical Report Overseas nº 2, January 1973, pp 49-57.

18. Johnson, R.F. and Sewell, Journal of the Iron and Steel Institute, December 1960, pp 414-444.

TABLE I

C(%)	Mn (%)	Si (%)	S (%)	P (%)	Mo (%)	Cr (%)	Ni (%)
1.01	0.27	0.14	0.002	0.009	0.02	1.45	0.05

TABLE II

Stress (MPa)	σ_x	σ_y	τ_{xy}	σ_Z	$\Delta\sigma$
Max	- 24.1	5.4	28.5	- 112	2120
Min	- 611	- 3070	- 66.8	- 1189	

TABLE III

Stress (MPa)	σ_x	σ_y	τ_{xy}	σ_Z	$\Delta\sigma$
Max	238	217	- 13.5	656	2510
Min	- 352	- 3610	- 392	- 1510	

TABLE IV

Stress (MPa)	Σ_x	Σ_y	T_{xy}	Σ_Z	θ^o	$\tau(t)$	$p(t)$
Max	- 24.1	5.43	28.1	- 112	45	14.7	- 43.5
Min	- 611	- 3070	-66.8	-1189	45	- 1229.5	-1623.3

TABLE V

Stress (MPa)	Σ_x	Σ_y	T_{xy}	Σ_Z	θ^o	$\tau(t)$	$p(t)$
Max	- 221	- 58.2	+ 144	- 561.4	45	81.4	- 280
	- 1040	- 4370	+ 11.3	- 2133.5	45	-1665	- 2514.5

TABLE VI

P_{max} MPa	Inclusion	Crack Initiation Life ($x\ 10^6$ cycles)		
		OKAMOTO (17)	JOHNSON (18)	Calculs
3500	Al_2O_3			260
3900	Al_2O_3		171 to 234	
5000	MnS	16 to 21.5		
	Al_2O_3	2.6 to 6.9		8.5
	$Si\ O_2$	13		
	Al_2O_3-FeO Al_2O_3-MnO	5.9 to 9		

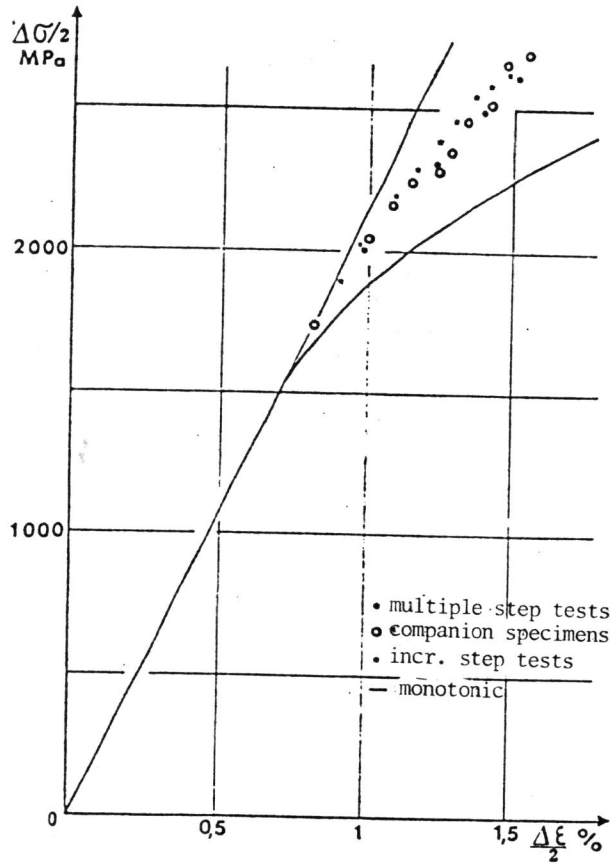

FIG. 1

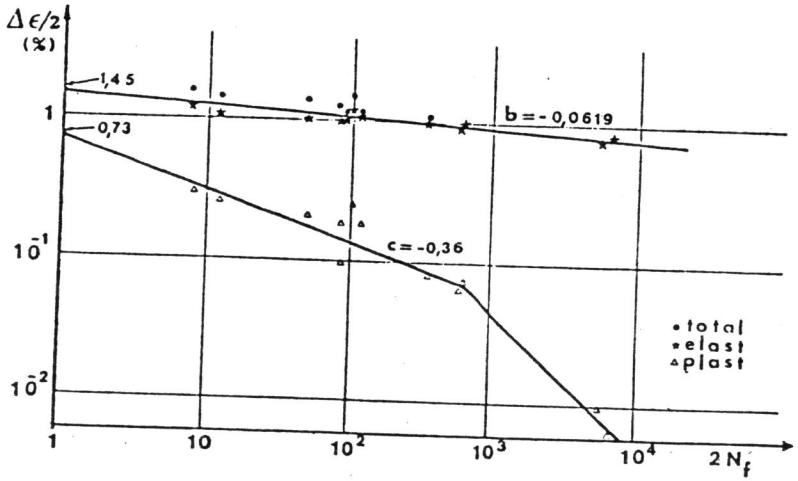

FIG. 2

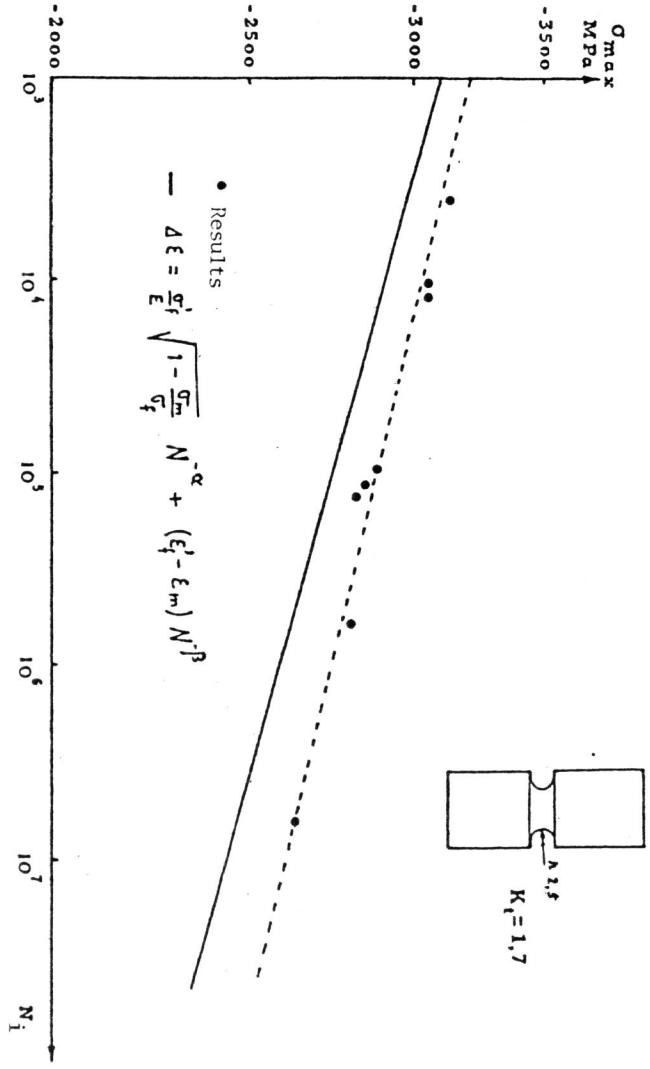

FIG. 3

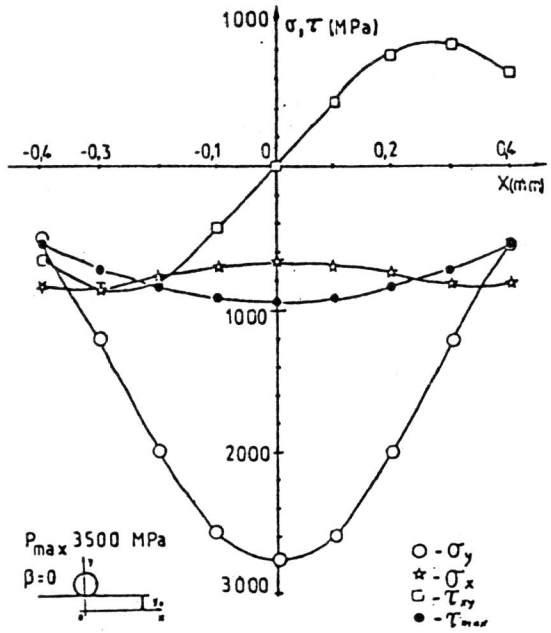

FIG. 4

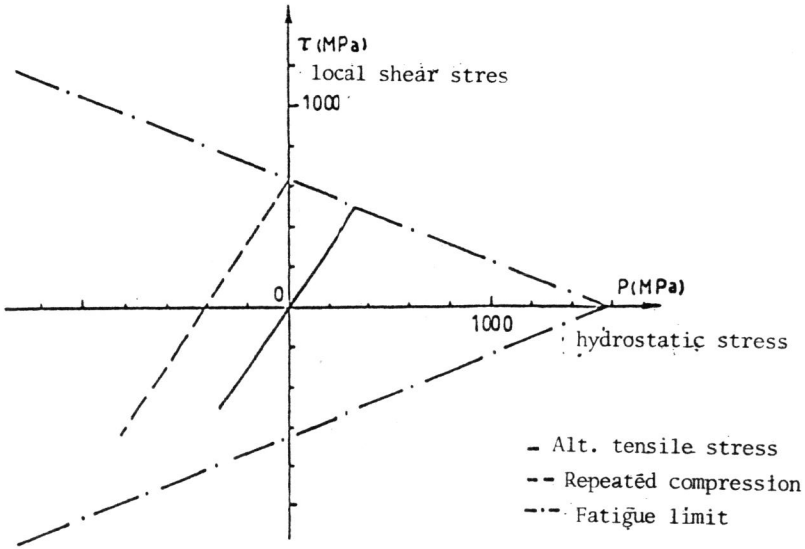

FIG. 5

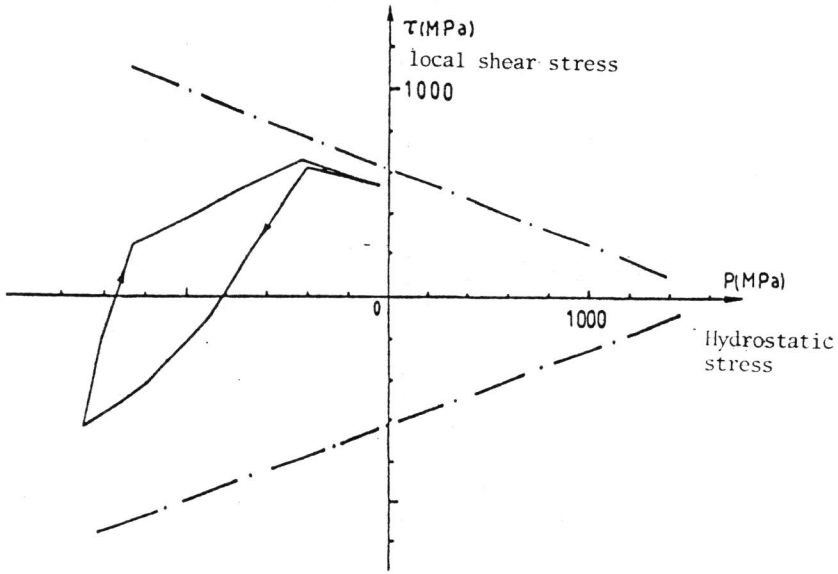
τ(MPa)
local shear stress
1000
P(MPa)
0
1000
Hydrostatic
stress

FIG. 6

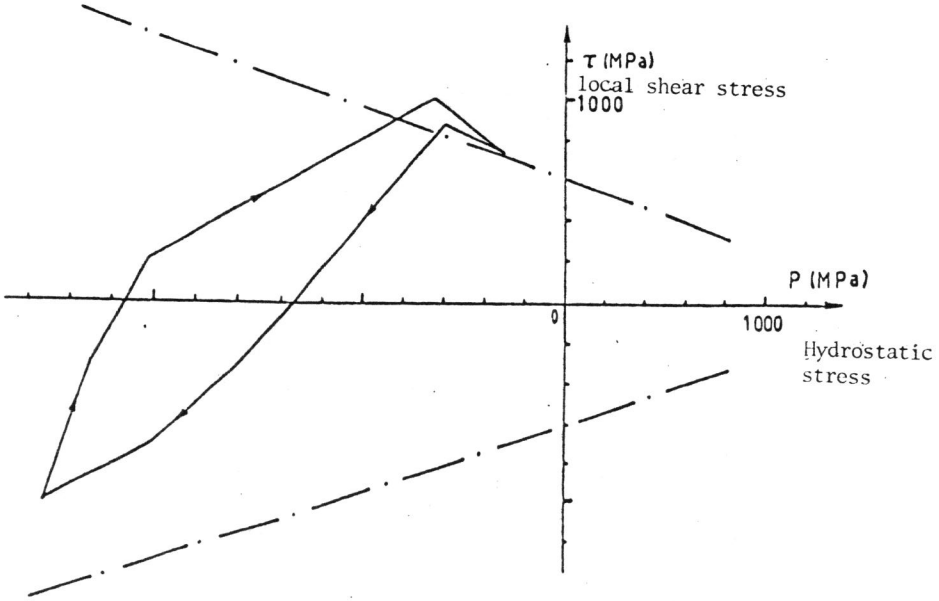
τ (MPa)
local shear stress
1000
P (MPa)
0
1000
Hydrostatic
stress

FIG. 7